ISSN- 2394-5125 VOL 07, ISSUE 09, 2020

Biological study on 1-(4'-chlorobenzoyl)-4-methyl-3-thiosemicarbazide and its Cu(II), Ni(II) binary chelates

Sandhepogu Thomas Leena Carlin[a] and B. Sirisha*

[a] Department of Chemistry, University College of science, Osmania University, Hyderabad – 500 007, (TS)India.

*E-mail: berleysiree@gmail.com

Abstract

Binary chelates of 1-(4'-chlorobenzoyl)-4-methyl-3-thiosemicarbazide (PCBMTSC, HL) with Cu(II) and Ni(II) ions have been synthesized and characterized by LC-MS, TGA, IR, UV-Visible analytical techniques. The spectral results suggested mononuclear nature for Ni(II), Cu(II)-PCBMTSC complexes. The optimized geometry, atomic charges, energies of HOMO, LUMO and energy gap, molecular electrostatic potential surface of PCBMTSC have been studied by DFT calculations using Gaussian 16W software. Equilibrium studies of 1-(4'-chlorobenzoyl)-4-methyl-3-thiosemicarbazide with Ni(II) ions was been carried out using Irving Rossotti titration technique, which revealed the monobasic nature of PCBMTSC and formation of 1:1 metal complex in the solution. Interaction of the metal chelates with calf thymus DNA has been evaluated using absorption spectroscopy, spectro-fluorimetry and viscosity measurements. The metal complexes exhibited hypochromism and intercalation mode of binding. The cleavage studies of metal complexes with supercoiled pBR33 DNA using gel electrophoresis method showed hydrolytic cleavage of plasmid DNA. The synthesized complexes also displayed antibacterial activity against Gram positive and Gram negative bacteria.

Keywords: Computational study, Equilibrium study, DNA interaction, DNA cleavage, antibacterial activity.

Introduction:

In last few decades heterocyclic compounds have contributed a major portion in improving the quality of life in terms of biological and industrial point of view due to their unique structures and properties. In nitrogen and sulphur containing heterocyclic compounds thiosemicarbazides and their derivatives have been focussed by researchers due to their wide spectrum of biological activities such as anticancer [1], anti-HIV [2], antifungal [3], antibacterial [4], antiamoebic [5] in mammalian cells as they posses the ability to penetrate through the cell membrane of disease causing micro-organisms.

Computational studies has been a successful predictive tool to study the properties of organic molecules such as ground state molecular geometries, quantum chemical properties, transition state energies, molecular potential energy surfaces [6]. Equilibrium studies assist in understanding the proton dissociation constant [7] of PCBMTSC and stability constant of its chelates with Co(II) and Ni(II) metal ions. Metal complexes have been used in various fields and drugs including metal ions exhibit higher activity than parent drug [8]. DNA has been primary target of most of anti-cancer drugs, DNA binding and cleavage studies help in understanding drug action which in turn supports to dent DNA and design less toxic and cheaper chemotherapeutic drugs [9]. The stability of metal complexes with therapeutic drugs plays an important role in their biological and chemical reactivity [10].

In view of enormous applications of thiosemicarbazides and their derivatives, the present study describes the synthesis, characterization, computational studies, equilibrium studies, DNA binding, DNA cleavage studies and antimicrobial activity of 1-(4'-chlorobenzoyl)-4- methyl-3-thiosemicarbazide and its Co(II), Ni(II) chelates.

Experimental

Materials and methods

4-methyl-3-thiosemicarbazide, parachlorobenzoylchloride, Calf Thymus DNA, Tris-HCl, NaCl and Ethidium Bromide were purchased from Sigma Aldrich, USA. Dimethylsulphoxide (DMSO), dimethylformamide (DMF) used for synthesis were purchased from Sisco Research Laboratory chemicals Mumbai. All the solvents and chemicals purchased were of analytical grade and used without any further purification methods. Magnetic moments of prepared complexes were determined using Guoy's method. Irving Rossetti pH titration technique has been used to determine the dissociation constant of ligand and stability constant of metal complexes. Buffer capsules of pH 4.00, 7.00 and 9.20 and metal salts were purchased from Merck, standardization of metal solutions was carried out by following the standard analytical method.[31]. Antimicrobial activity for the compounds was tested using Disc Diffusion method.

Instrumentation

Toshniwal hot stage apparatus and one end open capillary tubes were used to record melting points and presented uncorrected. LC-MS of the compounds were recorded on LC-MS 2010A Shimadzu spectrometer. Elemental studies were executed using 2400 CHN analyser (Perkin - Elmer). IR spectra were recorded on

ISSN- 2394-5125 VOL 07, ISSUE 09, 2020

Shimadzu Prestige-21 FTIR spectrophotometer in KBr disc. Electronic spectra were obtained in DMSO solution using Shimadzu UV 2450 spectrophotometer in the range of 200-1000nm. ^{1}H-NMR (with D_2O exchange) and ^{13}C-NMR spectra were recorded on Bruker WH-270MHz using TMS as internal standard and chemical shift in δppm. Thermogravimetric analyses were carried out on Perkin-Elmer model TGS-2 within the temperature range of 0ºC-1000ºC. Magnetic moments for solid complexes were calculated on Faraday balance model 7550. Equilibrium studies were carried out on a digital Elico (L1-120) pH meter using combined glass electrode. Conductance was measured on a Digisun digital conductivity meter mode D1 909 at room temperature in DMSO solution. DNA binding studies were carried out by UV absorption spectroscopy, using Schimazdu UV 3600 series spectrophotometer fluorescence emission spectra were recorded on RF-5301 spectrofluorophotometer, viscosity measurements were carried out using Ostwald's viscometer at a constant temperature of 303K. Computational studies for HL was performed using Gaussian 16W software.

Synthesis of 1-(4'chlorobenzoyl)-4-methyl-3-thiosemicarbazide (PCBMTSC):

Para chlorobenzoyl-3-thiosemicarbazide (0.015 Mol) in 10 mL of pyridine was added to 4-methylthiosemicarbazide (0.014 Mol) and the mixture solution was kept overnight at room temperature with continuous stirring. Oily residue was left after the removal of excess solvent. On cooling, the residue crystallized to colourless needles of 1-(4'-chlorobenzoyl)-4-methyl-3-thiosemicarbazide [11]. The purity of the compound was checked by TLC. Melting point was observed in the range of 194ºC-198ºC.

PCBMTSC: Yield: 65%; colour: white crystals; solubility: DMF, DMSO; Mp: 194°C -198°C; Mol. Wt: 243; Anal. Data calcd. (found) % for $C_9H_{10}N_3OS$: C, 44.53 (44.50); H, 4.12 (4.09); N, 17.32 (17.30). ^{1}H NMR: (δ, ppm): 10.44 (s, 1H, **NH**CS), 9.37 (s, 1H, CO**NH**), 8.17 (s, 1H, CH_3NH), 8.34(d, 1H, Ar-H), 8.13 (d, 2H, aromatic protons), 7.88 (d, 2H, aromatic protons), 2.87(d, 3H, C**H**$_3$). ^{13}CNMR: (δ, ppm): 182.35 (C=S), 165.04 (C=O), and 110-175 (Ar-C's). IR (KBr cm^{-1}): 3360 ($\nu_{\mathbf{NH}CH3}$), 3184 ($\nu_{CO\mathbf{NH}}$), 3121 ($\nu_{\mathbf{NH}CS}$), 2954(ν_{CH3}), 1670 ($\nu_{C=O}$), 1270($\nu_{C=S}$), 1246 and 1022 ($\nu_{H3\mathbf{C}\text{-}\mathbf{O}}$), 2491($\upsilon_{O\mathbf{CH3}}$) and 677($\upsilon_{C\text{-}Cl}$). UV-Vis (in DMSO): λ_{max} nm (cm^{-1}): 320 (31,250) π→π* of C=C(Ar), 260 (38387) n→π* (C=O), 227 (44052) n→π*(C=S). MS(m/z): 242[M-1]$^+$.

Synthesis of metal complexes:

The metal complexes have been synthesized by adding hot methanolic solution of PCBMTSC (25mL, 0.001mol, 0.250gm) to the metal chloride (0.0005 mol) [$CuCl_2.2H_2O$ (0.087g), $NiCl_2.6H_2O$ (0.118g)] solutions in 1:2 (M:L) molar ratio while stirring and the mixture was refluxed on water bath for 6 hours. pH of the solution was adjusted by adding few drops of methanolic ammonia buffer solution and further refluxed for 2 hours. Dark brown coloured Ni(II)-PCBMTSC and dark blue coloured Cu(II)-PCBMTSC complexes were separated out, washed with hot methanol to remove unreacted ligand followed by double distilled water to remove unreacted metal salt. Further the metal complexes were washed with petroleum ether and dried over anhydrous $CaCl_2$ at room temperature under vacuum for 24 hours. Purity of the complexes had been checked using TLC.

[Ni (PCBMTSC)$_2$(H_2O)$_2$] (**1**)

Yield: 68%; colour: dark brown; Dp: above 300°C; solubility: DMF, DMSO; conductivity measurement: < 18 ohm^{-1}cm^{2}mol^{-1}; Anal. Data calcd. (found)% for [Ni(PCBMTSC)$_2$(H_2O)$_2$]: C, 37.24 (37.20); H, 2.24 (2.21); N, 14.8 (14.5); M, 10.12 (10.09); μ_{eff} (BM): 2.78; IR (KBr, cm^{-1}): 1562 ($\nu_{C=N}$), 1147 ($\nu_{C\text{-}O}$), 570-550 ($\nu_{Ni\text{-}N}$), 410-380 ($\nu_{Ni\text{-}O}$). Electronic spectra: λ_{max} (cm^{-1}): 10,028 ($^3A_{2g}\rightarrow{}^3T_{2g(F)}$), 16,850 ($^3A_{2g}\rightarrow{}^3T_{1\ g(F)}$), 26,500 ($^3A_{2g}\rightarrow{}^3T_{1g\ (P)}$). MS(m/z): 579 [M-1]$^+$.

[Cu (PCBMTSC)$_2$ (H_2O)$_2$] (**2**)

Yield: 71%; colour: dark blue; Dp: above 300°C; solubility: DMF, DMSO; conductivity measurement: < 20 ohm^{-1}cm^{2}mol^{-1}; Anal. Data calcd. (found) % for [Cu(PCBMTSC)$_2$(H_2O)$_2$]: C, 36.93(36.89); H, 3.76 (3.74) 3.84; N, 14.36 (14.32); M, 10.85(10.80); μ_{eff} BM: 1.87. IR (KBr, cm^{-1}): 1571($\nu_{C=N}$), 1089 ($\nu_{C\text{-}O}$), 570-550 ($\nu_{Cu\text{-}N}$), 450-420 ($\nu_{Cu\text{-}O}$); Electronic spectra λ_{max} (cm^{-1}): 15,152 ($^2B_{1g}\rightarrow{}^2A_{1g}$), 25,125 ($^2B_{1g}\rightarrow{}^2B_{2g}$), 29,154 ($^2B_{1g}\rightarrow{}^2E_g$). MS(m/z): 584 [M-1]$^+$.

ISSN- 2394-5125 VOL 07, ISSUE 09, 2020

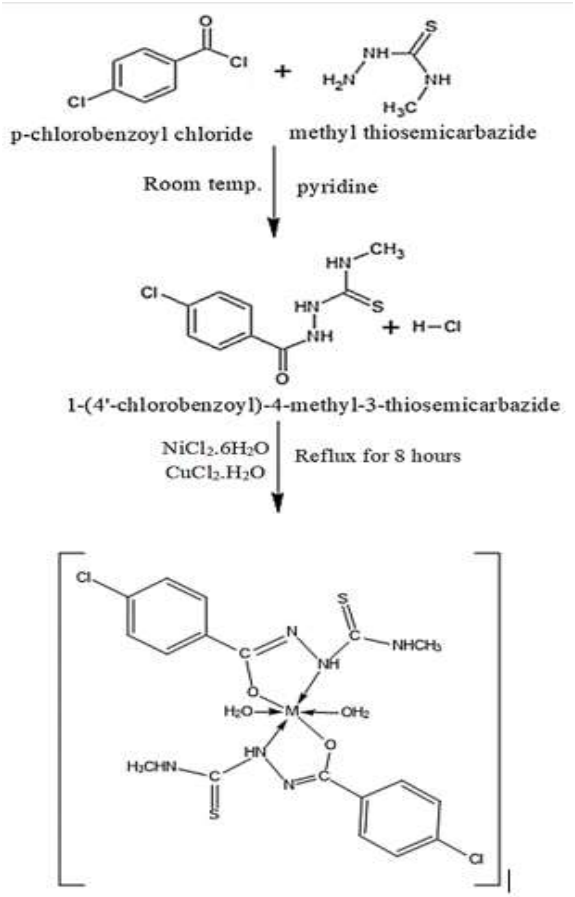

[M= Ni(II), Cu(II)-PCBMTSC]

Scheme-I: Synthesis of HL and its chelates with Ni(II), Cu(II) ions

Computational calculations:

Computational calculations of HL had been carried out using Gaussian 16W program. The Density functional theory (DFT) was used to determine chemical structures of molecules and structural changes in molecules. The geometry optimization of the compound was carried out using closed-shell Becke-Lee-Yang-Parr hybrid exchange-correlation three parameter functional (B3LYP) in combination with 6-311G(d,p) basis set [12,13]. After the completion of optimization, the theoretical properties of the compound such as free energy, heat of formation, HOMO and LUMO were recorded. HOMO and LUMO surfaces and molecular electrostatic potential mapping has been generated.

The Energy difference between HOMO and LUMO orbitals called as energy gap has been a key parameter that determines the stability, molecular electrical transport properties of the compounds. A molecule with a small gap shows high chemical reactivity, low kinetic stability and is termed as soft molecule and a molecule with large gap shows high electron affinity, acts as electron acceptor and termed as hard molecule.

$$Egap = (E_{LUMO} - E_{HOMO}) \approx IP - EA$$

The energy of HOMO is directly related to ionization potential and the energy of LUMO is related to the electron affinity of the molecule. The energies of HOMO and LUMO were used for the determination of global reactivity descriptors. These are electrophilicity (ω), chemical potential (μ), electronegativity (χ), hardness (η), softness (S) and additional electronic charge (ΔNmax) which can be calculated from the following equations,

$(\mu) = -I+A/2$; $(\eta) = I-A/2$; $(S) = 1/\eta$; $(\chi) = I+A/2$; $(\omega) = \mu^2/2\eta$; $\Delta Nmax = -\mu/\eta$

Equilibrium studies:

The acid dissociation constant of HL and the formation constant of Ni(II) ions with HL in solution have been determined by performing potentiometric pH titrations in 70% v/v DMF-water medium at 303K and 0.1M (KNO_3) ionic strength using Irving Rossotti titration technique [14]. The technique involves the titration of the following sets of solutions against 0.1M standard base solution.

a. HNO_3 (4.0×10^{-3}M)

b. HNO_3 (4.0×10^{-3}M) + Ligand (1.0×10^{-3}M)

c. HNO_3 (4.0×10^{-3}M) + Ligand (1.0×10^{-3}M) + Metal ion (2.0×10^{-4}M)

ISSN- 2394-5125 VOL 07, ISSUE 09, 2020

After the titration is finished, graphs were plotted taking volume of alkali added on x-axis and observed pH values on y-axis resulting in different titration curves. The trend observed in the titration curves was different. The curves obtained were the acid curve (A), the ligand curve (A+L) and the metal chelate curve (A+L+M). The titration curves, indicating the complexation. We can calculate the average number of protons associated per ligand ($\bar{n}_A$), the number of metal ligand complexes ($\bar{n}$) and pL (Free Ligand exponent) from the graphs.

$$\bar{n}_A = \frac{\text{Total concentration of proton bound to ligand}}{\text{Total concentration of ligand not bound to metal ion}}$$

$$\bar{n} = \frac{\text{Total concentration of ligand not bound to metal ion}}{\text{Total concentration of metal ion}}$$

$$\bar{n}_A = \left[YT_L^o + \left\{ \frac{(V_1 - V_2)(N + E^o)}{(V_0 + V_1)} \right\} \right] \Big/ T_L^o$$

$$pL = \log \frac{\sum_{j=0}^{j=j} \beta_J^H \left(\frac{1}{\text{anti log pH}} \right)^J}{(T_L^o - \bar{n} T_M^o)} * \frac{V_0 + V_3}{V_0}$$

Here,

Y = No. of dissociable protons present in the ligand

T_L^o = Total ligand concentration

T_M^o = Metal ion concentration

N = Concentration of base

V_0 = Total initial volume

V_1, V_2, V_3 = Volumes of alkali consumed to reach a given pH value on the titration curve of acid, ligand and metal respectively.

β_J^H = Successive overall proton-ligand formation constant

The pH value at 0.5 $\bar{n}_A$ corresponds to the pKa of ligand, it can be accurately calculated by the method of linear plot relationship, $LogK_H$ = pH-Log (1- $\bar{n}_A$)/ $\bar{n}_A$. If $\bar{n}$ value is 0.5, 1.5 it corresponds to formation of 1:1 and 1:2 complexes respectively. The intercept values of Log (1- $\bar{n}$)/ $\bar{n}$ vs pL and Log (2- $\bar{n}$)/($\bar{n}$ -1) vs pL gives $LogK_1$ (1:1) and $LogK_2$ (1:2) respectively.

DNA binding studies:

UV-Visible absorption studies: Tris HCl/NaCl buffer (50mM Tris HCl/5mM NaCl buffer; pH 7.2) and (10%) of metal complex solutions in DMSO were used to perform DNA binding experiments. Using the absorption intensity at 260nm with ε value of $6600M^{-1}$ cm^{-1} calf thymus (CT) DNA concentration was determined. Keeping the concentration of complex constant, and varying the concentrations of CT DNA (20, 40, 60, 80, 100μM) absorption titration experiments were carried out. Using the equation [15] [DNA] / (ε_a- ε_f) = [DNA] / (ε_b- ε_f) +1 /Kb(ε_b- ε_f), where $\varepsilon_a = A_{obs}$/ [complex], ε_f and ε_b being the extinction coefficients for free (unbound) and fully bound complex forms respectively.

Fluorescence studies: The quenching of the EtBr-DNA adduct fluorescence has been studied by observing the emission spectra of the metal complexes of PNBTSC in the wavelength range of 530-770 nm with an excitation wavelength of 520 nm, upon addition of different metal complex concentrations to DNA pre-treated with EB. The fluorescence quenching at around 590-610nm can be described by the equation: $I_o/I = 1 + K_{sv}r$ [16-18] where I_o and I are the fluorescence intensities the DNA-EB adduct in the absence and in the presence of complex respectively, K_{sv} is a linear Stern–Volmer quenching constant, and r is the ratio of the total concentration of complex to that of DNA. There are three types of quenching based on I_0/I versus [r] plot. When the I_0/I versus [r] plot is linear the type of quenching is either dynamic or static quenching; or it may be a combination of both [19]. Static quenching is decrease in stability of complexes with the increase in temperature and the opposite is dynamic quenching [20].

Viscosity measurement: Viscosity is dependent on the change in the length of DNA on the addition of potential binding species. When a metal complex binds by intercalation, it causes the separation of base pairs in the structure of DNA, resulting in the lengthening of DNA helix and increase in its viscosity. Ostwald's viscometer was used for measurements maintaining 303K with the help of thermostatic bath [21]. Stock solutions of metal complexes have been prepared in DMSO and diluted to 50μM using Tris HCl buffer. 10mL of buffer, 100μL of CT-DNA (200 μM) were taken in the viscometer and complex solution was added with an increment of 20μL each time from 0 -100 μL. The flow time of each sample was measured in triplicate using a stop clock and the average flow time was noted. Viscosity values were calculated with the observed flow time of a DNA solution

ISSN- 2394-5125 VOL 07, ISSUE 09, 2020

(t), corrected with the flow time of the buffer alone (t_0). To study the effect of DNA binding on the viscosity of the complex, the results were plotted $(\eta/\eta_0)^{1/3}$ versus [complex]/[DNA], where η has been the viscosity of DNA in the presence of the metal complex and η_0 the viscosity of the DNA alone. η and η_0 were calculated by using the equations: $\eta = (t_1 - t_0)/ t_0$ and $\eta_0 = (t - t_0)/ t_0$, where t_0 = flow time of the buffer solution alone, t = flow time of DNA solution in the absence of complex and t_1 = flow time of DNA solution in the presence of complex.

DNA cleavage studies: In the process of DNA cleavage, plasmid DNA is converted from super coiled DNA (Form I) to nicked circular (Form II) and linear forms (Form III) [22]. In the experiment, pBR33 DNA (300 ng/3 µL) has been mixed with the complexes in DMSO (20-60 µM) in 5 mM Tris. HCl/50 mM NaCl buffer (pH 7.2). The mixture was incubated at 37ºC for 1 hour and added with loading buffer containing 1% bromophenol blue and 40% sucrose (1 µL) and was loaded upon 0.8% agarose gel containing EB (1 µg/mL). In TAE buffer (40 mM Tris base, 20 mM acetic acid, 1 mm EDTA, pH 8.3) the gel was run at a constant voltage 60 V for 2 h until the bromophenol blue travels through 75% of the gel. The bands obtained have been visualized by viewing the gel on a transilluminator and photographed.

Antimicrobial studies: The Kirby-Bauer disc diffusion method [23] was employed for the study of antimicrobial effects of PCBMTSC and its chelates with Ni(II), Cu(II) ions against *Bacillus subtilis* (gram+ve) and *Escherichia coli* (gram-ve) bacteria with a concentration of 50µg/mL in DMSO. Sterile discs impregnated with a defined quantity of antimicrobial agent are placed on agar plates uniformly seeded with 5µL of test sample. If the test sample is microbially active an inhibition zone is developed around the disc. The zone of inhibition was recorded in mm for all the compounds after incubating the samples for 24 hours at 310K, using Gentamycin as standard [24].

Results and Discussion

Characterization of PCBMTSC and its metal complexes 1 and 2

Physical and analytical data of synthesized compounds: PCBMTSC was white in colour, crystalline at room temperature, non-hygroscopic and soluble in methanol, DMF, DMSO. Physical and analytical data of HL and its chelates have been presented Table 1. The conductance values [25] of complexes 1 and 2 were less than 8 $ohm^{-1}\ cm^2\ mol^{-1}$ indicating their non-electrolytic nature. Absence of chloride in complexes has been confirmed by the negative result in Volhard's test.

Table 1: Physical and analytical data of HL and its chelates 1 and 2

Compound	Color (Yield%)	M.P ºC	Found (calc.)			
			C	H	N	M
HL	White (65)	194 - 198	44.50 (44.53)	4.09 (4.12)	17.30 (17.32)	-
1	Dark Brown (68)	Dp	37.20 (37.24)	2.21 (2.24)	14.45 (14.48)	10.09 (10.12)
2	Dark Blue (71)	Dp	36.89 (36.92)	3.74 (3.76)	14.32 (14.36)	10.80 (10.85)

LCMS: The liquid chromatograms of Ni(II)-PCBMTSC and Cu(II)-PCBMTSC showed a single peak indicating the purity of the complex. The mass spectrum of Ni(II)-PCBMTSC complex showed molecular ion peak at m/z 579 attributed to $[NiL_2(H_2O)_2]^+$ indicating the formation of 1:2 metal- ligand complex. Peaks at m/z 544 $[NiL_2]^+$, m/z 300 $[Ni(L)]^+$, m/z 264 $[Ni(C_9H_9N_3OS)]^+$ and m/z 58 $[Ni]^+$ have also been observed. Cu(II)-PSBMTSC complex displayed a molecular ion peak in the mass spectrum at m/z 584 $[CuL_2(H_2O)_2]^+$ indicating 1:2 ratio of complex. The mass spectrum also showed peaks at m/z 547 $[CuL^2]^+$, m/z 517 $[Cu(C_{16}H_{12}N_6O_2S_2Cl_2)]^+$, m/z 446 $[Cu(C_{16}H_{12}N_6O_2S_2)]^+$ and m/z 63 $[Cu]^{+\cdot}$

Thermogravimetric analyses: Decomposition of Ni(II)-PCBMTSC complex (Figure 1) occurred in four steps. The weight loss in the first step was 7.26% from 190^0C to 270^0C due to the loss of two moles of coordinated water. Major portion of the complex moiety decomposed in the next two steps from 290^0C-500^0C about 64%, in the fourth step weight loss was 4.06% with 24.8% of residue reveal partial decomposition of chelate.

Cu(II)-PCBMTSC complex (Figure 2) undergoes decomposition in three steps. In the first step, gradual weight loss of 5.95% from 100^0C to 260^0C was due to loss of two coordinated water molecules. In the second step a sudden decrease of weight about 60% corresponding to complex moiety then gradual decomposition of 5.8% was noticed with 30% residue which reflects the partial decomposition of the complex.

ISSN- 2394-5125 VOL 07, ISSUE 09, 2020

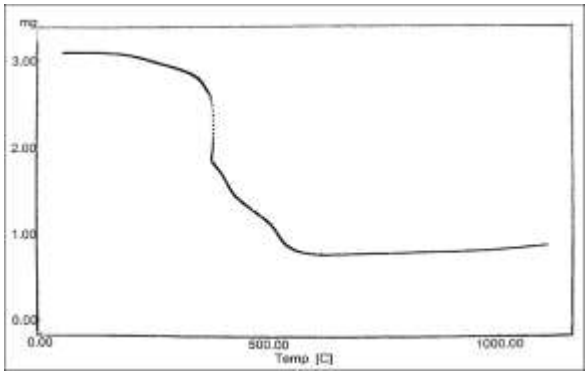

Fig. 1. Thermogram of Ni(II)-PCBMTSC complex

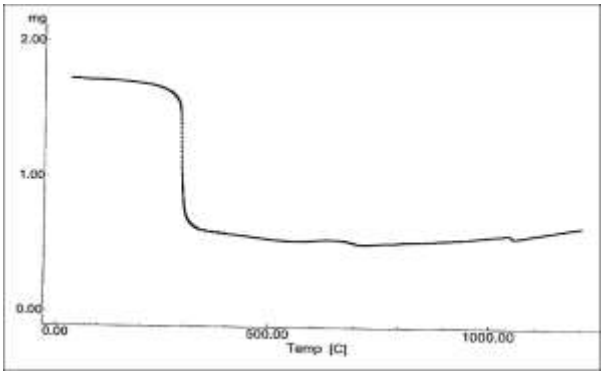

Fig. 2. Thermogram of Cu(II)-PCBMTSC complex

IR spectra:IR spectra of Ni(II) and Cu(II)-PCBMTSC complexes (Figures 3,4) showed a broad band above 2900 cm^{-1} due to the presence of coordinated water molecules. Peaks corresponding to υ_{N1-H} at 3184 cm^{-1} and $\upsilon_{C=O}$ at 1670 cm^{-1} in IR spectrum of ligand have vanished in the complex spectra and new bands at 1562 cm^{-1}, 1571 cm^{-1} corresponding to $\upsilon_{C=N}$, peaks at 1147 cm^{-1}, 1089 cm^{-1} corresponding to υ_{C-O} in their respective metal complex spectra were observed indicating keto-enol tautomerism and ligand binds with metal ion in enol form after deprotonation. Variation in the stretching frequency value of υ_{N2-H} also reveals the binding of enolic oxygen and N2 with corresponding metal ions to result five membered chelates. In the Far IR region bands at 550-530cm^{-1} (υ_{M-N}), 470-420cm^{-1} (υ_{M-O}), 320-280cm^{-1} (υ_{M-OH2}) were present respectively.

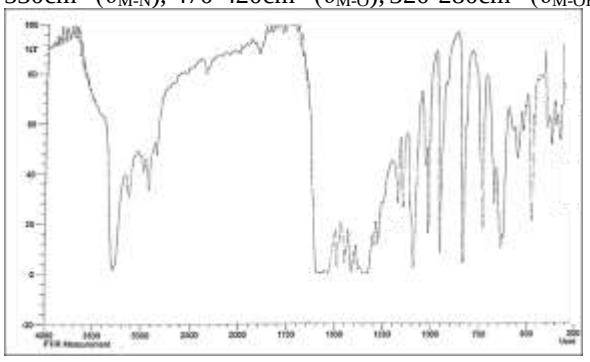

Fig. 3. IR spectrum of Ni(II)-PCBMTSC complex

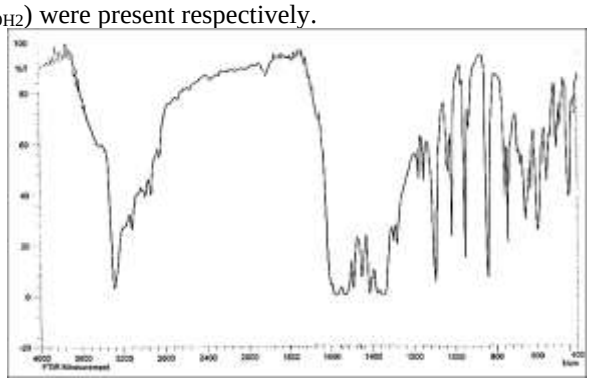

Fig. 4. IR spectrum of Cu(II)-PCBMTSC complex

ESR spectra: ESR spectra for Ni(II) and Cu(II)-PCBMTSC complexes has been recorded at room temperature (Figures 5, 6). The Spin-Hamiltonian parameters for both the metal complexes has been calculated and given in the Table 2.

ESR studies of Ni(II)-PCBMTSC at room temperature displayed G value lower than 5 reflecting that exchange interaction is considerable and local tetragonal axes have been misaligned. The ESR spectrum of Cu(II)PCBMTSC shows G value greater than 5 indicating the negligible interaction as the local tetragonal axes may aligned parallel. The value of bonding parameter α^2 in Cu(II) complexes has been in the range of 0.81-0.99, reveals the covalent character of metal-ligand bond. In all the complexes the orbital reduction factors K$\parallel$ and K$^{\perp}$ follow the trend K$\parallel$ >K$^{\perp}$ suggesting the considerable out -of -plane π-bonding.

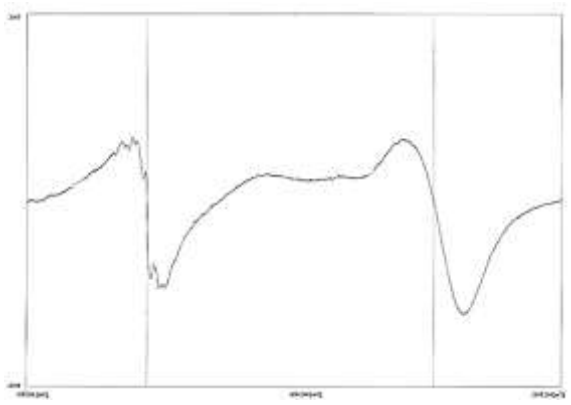

Fig. 5.ESR of Ni(II)-PCBMTSC complex

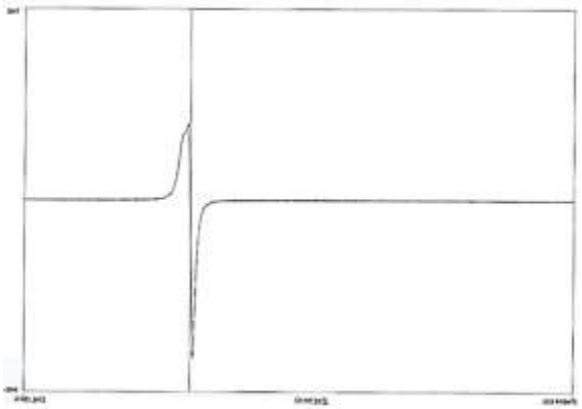

Fig. 6. ESR spectrum of Cu(II)-PCBMTSC complex

ISSN- 2394-5125 VOL 07, ISSUE 09, 2020

Table 2: Spin Hamiltonian parameters of complexes 1 and 2

Complex	$g_{\parallel}$	$g^{\perp}$	G	$A_{\parallel}$ x10^{-4} cm^{-1}	α^2	β^2	γ^2	$K_{\parallel}$	$K^{\perp}$
1	2.18	2.05	3.53	38.6	0.34	2.19	1.18	1.21	0.53
2	2.15	2.03	5.30	67.5	0.99	0.31	0.25	0.37	0.12

Magnetic susceptibility

The magnetic moment value of Ni(II)-PCBMTSC and Cu(II)-PCBMTSC complexes [26] has been found to be 2.78 BM and 1.87 BM respectively corresponding to two and one unpaired electron respectively.

UV-Visible spectra

The UV- Visible spectrum of Ni(II)-PCBMTSC complex (Figure 7) showed the transitions for $^3A_{2g}(F) \rightarrow {}^3T_{2g}(F)$ (12,208 cm^{-1}), $^3A_{2g}$ (F) $\rightarrow {}^3T_{1g}$ (F) (16,850 cm^{-1}), and $^3A_{2g}$ (F)$\rightarrow {}^3T_{1g}$ (P) (26,500 cm^{-1}) corresponding to octahedral geometry [27] of the complex.

The d-d transitions observed in the UV- Visible spectrum of the Cu(II)-PCBMTSC[32,33] complex (Figure 8) were $^2B_{1g}\rightarrow {}^2E_g$ (27,235 cm^{-1}), $^2B_{1g}\rightarrow {}^2B_{2g}$ (16150 cm^{-1}), $^2B_{1g}\rightarrow {}^2A_{1g}$ (13,100cm^{-1}), ans charge transfer transition at 36,921 cm^{-1} indicating the distorted octahedral structure. UV-Visible spectral data of PCBMTSC and its chelates have been tabulated in Table 3.

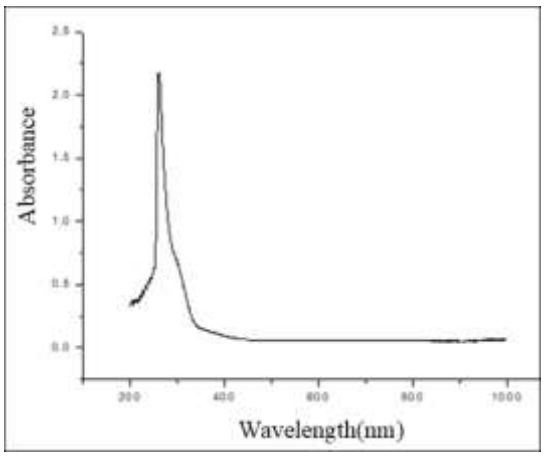

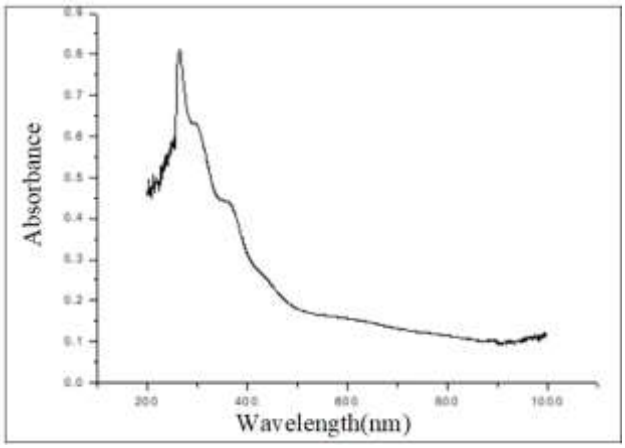

Fig.7. UV-Visible spectrum of Ni(II)-PCBMTSC **Fig.8. UV-Visible spectrum of Cu(II)-PCBMTSC**

Table 3. UV-Visible spectra of HL and its chelates

Compound	Absorbance (cm^{-1})	Band assignment	υ_2/υ_1	υ_3/υ_1	Dq (cm^{-1})	β	B (cm^{-1})	Proposed geometry
HL	31,250 38387 44,052	π→π*(C=C) n→π*(C=O) n→π*(C=S)	-	-	-	-	-	-
1	12,028 16,850 26,500 37,543	$^3A_{2g}\rightarrow {}^3T_{2g}(F)$ $^3A_{2g}\rightarrow {}^3T_{1g}(F)$ $^3A_{2g}\rightarrow {}^3T_{1g}(P)$ CT band	1.40	2.20	1202.8	0.45	484.4	Distorted Oh
2	15,152 25,125 29,154 36,921	$^2B_{1g}\rightarrow {}^2A_{1g}$ $^2B_{1g}\rightarrow {}^2B_{2g}$ $^2B_{1g}\rightarrow {}^2E_g$ CT band	1.23	2.07	305.0	-	-	Distorted Oh

Computational studies

Computed data of 1-(4'-chlorobenzoyl)- 4-methyl-3-thiosemicarbazide (PCBMTSC): From ^{1}H-NMR spectrum the compound 1-(4'-chlorobenzoyl)-4-methyl-3-thiosemicarbazide there has been evidence for keto enol tautomerism and the following keto enol and thione thiol forms were possible for the compound and showed in Figure 9.

ISSN- 2394-5125 VOL 07, ISSUE 09, 2020

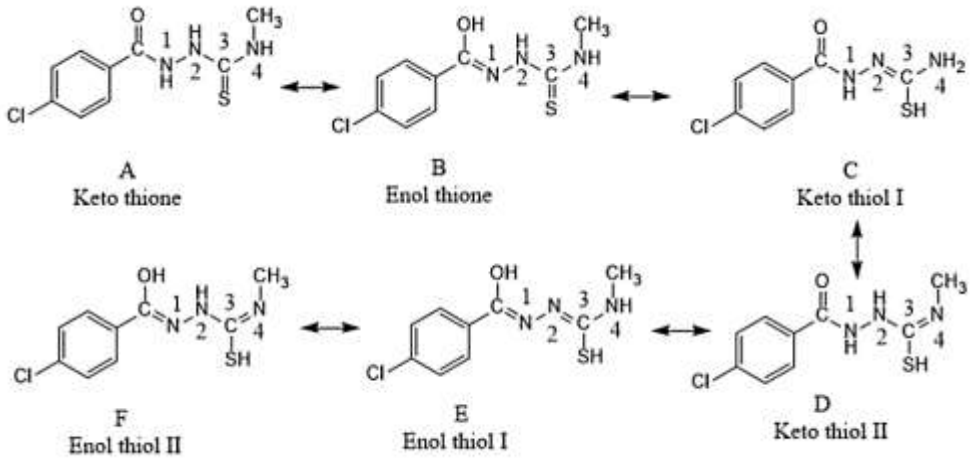

Figure 9. Keto enol and thione thiol tautomerism in PCBMTSC

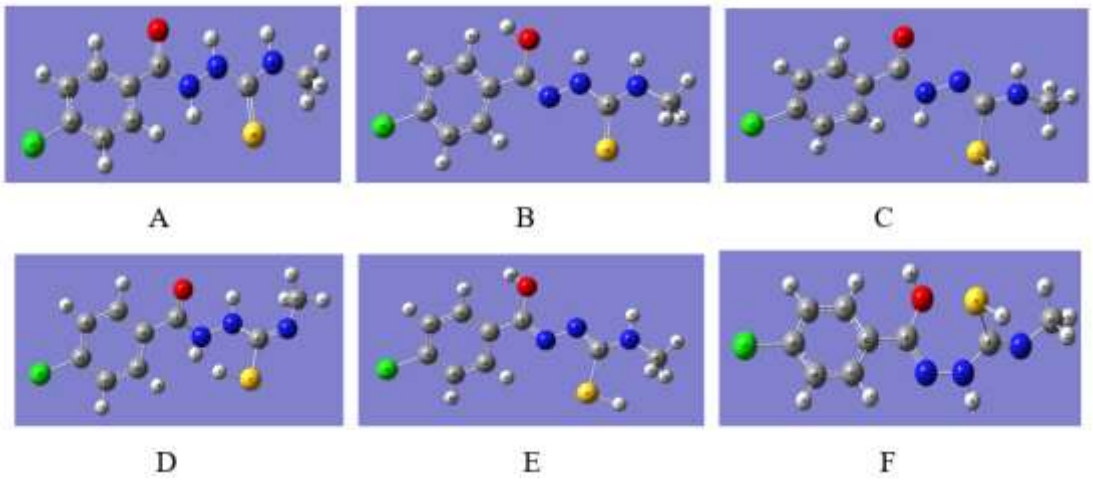

Figure 10. Optimized structures of A-F forms of PCBMTSC

The DFT optimized geometries of all the forms of the compound PCBMTSC were given in Figure 10, in this compound 25 atoms were present.

Table 4: Thermodynamic properties of A-F forms of PCBMTSC

Properties	**A**	**D**	**C**	**D**	**E**	**F**
Total energy (kcal/mol)	-907798	-907781	-907774	-907768	-907760	-907753
Entropy (kcal/mol-kelvin)	0.12771	0.12729	0.12935	0.13157	0.13011	0.12915
Enthalpy (kcal/mol)	-907760	-907743	-907736	-907729	-907722	-907714
Free energy (kcal/mol)	-907798	-907781	-907774	-907768	-907760	-907753
Heat capacity (kcal/mol-kelvin)	0.05432	0.05930	0.05547	0.05586	0.05623	0.05675
Dipole moment, (D)	3.81395	7.21176	5.39220	3.82623	4.35784	2.12106
RMS gradient (kcal/mol)	0.01144	0.00383	0.00564	0.00544	0.01258	0.00160
Electronic energy (kcal/mol)	-907888	-907870	-907861	-907739	-907846	-907838

Table 5: Mulliken charges on the atoms of A-F forms of PCBMTSC

A	**B**	**C**	**D**	**E**	**F**

ISSN- 2394-5125 VOL 07, ISSUE 09, 2020

1 N -0.495923	1 N -0.125590	1 N -0.586993	1 N -0.541946	1 N -0.285382	1 N -0.179784
2 H 0.394057	2 N -0.571840	2 H 0.363643	2 H 0.358798	2 N -0.283605	2 N -0.516354
3 N -0.473968	3 H 0.336221	3 N -0.119565	3 N -0.438880	3 C 0.245027	3 H 0.352142
4 H 0.369497	4 C 0.286215	4 C 0.131625	4 H 0.351157	4 N -0.626543	4 C 0.205790
5 C 0.273345	5 N -0.650891	5 N -0.588590	5 C 0.134460	5 H 0.349798	5 S -0.039650
6 N -0.654641	6 H 0.319877	6 H 0.336394	6 S 0.049236	6 S 0.046611	6 H 0.109434
7 H 0.329862	7 C 0.388241	7 S -0.052589	7 H 0.114403	7 H 0.099368	7 N -0.328624
8 C 0.513393	8 O -0.635493	8 H 0.137785	8 N -0.282527	8 C 0.426528	8 C 0.425867
9 O -0.457960	9 H 0.390641	9 C 0.536934	9 C 0.494829	9 O -0.564281	9 O -0.592793
10 S -0.154879	10 S -0.083792	10O -0.381082	10O -0.396403	10 H 0.371039	10 H 0.391540
11C -0.133553	11 C -0.103103	11 C -0.158489	11 C -0.149557	11 C -0.140999	11 C -0.123188
12C -0.055327	12 C -0.118676	12 C -0.090071	12 C -0.077820	12 C -0.129418	12 C -0.118571
13C -0.092945	13 C -0.049617	13 C -0.099971	13 C -0.088557	13 C -0.050056	13 C -0.053137
14C -0.086467	14 C -0.079655	14 C -0.078837	14 C -0.075802	14 C -0.075260	14 C -0.073695
15 H 0.183051	15 H 0.166188	15 H 0.177598	15 H 0.180513	15 H 0.170636	15 H 0.176548
16C -0.063745	16 C -0.078331	16 C -0.058939	16 C -0.059861	16 C -0.078290	16 C -0.073686
17 H 0.198466	17 H 0.223678	17 H 0.195897	17 H 0.200013	17 H 0.210848	17 H 0.189502
18C -0.274278	18 C -0.273486	18 C -0.280089	18 C -0.279320	18 C -0.275904	18 C -0.276769
19 H 0.193808	19 H 0.189286	19 H 0.189410	19 H 0.195615	19 H 0.187684	19 H 0.189951
20 H 0.194310	20 H 0.195561	20 H 0.192492	20 H 0.197862	20 H 0.189846	20 H 0.191486
21Cl -0.006824	21Cl -0.011330	21Cl -0.014028	21 Cl 0.001107	21Cl -0.018907	21Cl -0.013766
22C -0.332540	22 C -0.329954	22 C -0.353867	22 C -0.459082	22 C -0.379078	22 C -0.430453
23 H 0.230315	23 H 0.224581	23 H 0.192994	23 H 0.194278	23 H 0.204600	23 H 0.188810
24 H 0.173106	24 H 0.164986	24 H 0.215868	24 H 0.208993	24 H 0.193932	24 H 0.201001
25 H 0.229842	25 H 0.226281	25 H 0.192470	25 H 0.168492	25 H 0.211807	25 H 0.198401

Table 6: Optimized geometric parameters of form A of PCBMTSC

Bond length (Å)		**Bond angles(Å)**		**Dihedral angles(Å)**	
R(1,2)	1.0124	A(2,1,3)	113.6647	D(2,1,3,4)	173.9823
R(1,3)	1.3925	A(2,1,8)	128.7991	D(2,1,3,5)	-4.6272
R(1,8)	1.362	A(3,1,8)	117.2207	D(8,1,3,4)	-0.1396
R(3,4)	1.0133	A(1,3,4)	111.6795	D(8,1,3,5)	-178.7491
R(3,5)	1.3592	A(1,3,5)	121.5442	D(2,1,8,9)	-172.1845
R(5,6)	1.3572	A(4,3,5)	126.7597	D(2,1,8,11)	7.227
R(5,10)	1.7402	A(3,5,6)	114.973	D(3,1,8,9)	0.9027
R(6,7)	1.0087	A(3,5,10)	121.5737	D(3,1,8,11)	-179.6858
R(6,22)	1.4638	A(6,5,10)	123.453	D(1,3,5,6)	-179.5269
R(8,9)	1.2634	A(5,6,7)	118.9893	D(1,3,5,10)	0.6714
R(8,11)	1.4841	A(5,6,22)	123.6333	D(4,3,5,6)	2.0861
R(11,12)	1.4041	A(7,6,22)	117.3747	D(4,3,5,10)	-177.7156
R(11,13)	1.4026	A(1,8,9)	119.370	D(3,5,6,7)	1.1577
R(12,14)	1.3951	A(1,8,11)	117.5877	D(3,5,6,22)	-179.4573
R(12,15)	1.0817	A(9,8,11)	123.039	D(10,5,6,7)	-179.0447
R(13,16)	1.3937	A(8,11,12)	123.3649	D(10,5,6,22)	0.3402
R(13,17)	1.08	A(8,11,13)	117.3112	D(5,6,22,23)	59.7147
R(14,18)	1.3905	A(12,11,13)	119.3145	D(5,6,22,24)	179.5136
R(14,19)	1.0791	A(11,12,14)	120.489	D(5,6,22,25)	-60.6299
R(16,18)	1.3908	A(11,12,15)	121.1293	D(7,6,22,23)	-120.8911
R(16,20)	1.0792	A(14,12,15)	118.3604	D(7,6,22,24)	-1.0922
R(18,21)	1.8257	A(11,13,16)	120.6705	D(7,6,22,25)	118.7642
R(22,23)	1.0892	A(11,13,17)	118.5398	D(1,8,11,12)	16.9415
R(22,24)	1.088	A(16,13,17)	120.7893	D(1,8,11,13)	-164.1808
R(22,25)	1.08	A(12,14,18)	118.7427	D(9,8,11,12)	-163.670
		A(12,14,19)	120.7223	D(9,8,11,13)	15.2075
		A(18,14,19)	120.5327	D(8,11,12,14)	179.8269
		A(13,16,18)	118.6597	D(8,11,12,15)	1.534
		A(13,16,20)	120.8384	D(13,11,12,14)	0.9705

ISSN- 2394-5125 VOL 07, ISSUE 09, 2020

	A(18,16,20)	120.501	D(13,11,12,15)	-177.3224
	A(14,18,16)	122.1147	D(8,11,13,16)	-179.9487
	A(14,18,21)	118.8835	D(8,11,13,17)	-0.1942
	A(16,18,21)	119.000	D(12,11,13,16)	-1.0236
	A(6,22,23)	110.8988	D(12,11,13,17)	178.7309
	A(6,22,24)	108.0407	D(11,12,14,18)	-0.2527
	A(6,22,25)	110.9707	D(11,12,14,19)	-179.7053
	A(23,22,24)	109.327	D(15,12,14,18)	178.0868
	A(23,22,25)	108.2424	D(15,12,14,19)	-1.365
	A(24,22,25)	109.3395	D(11,13,16,18)	0.3551
			D(11,13,16,20)	-179.7159
			D(17,13,16,18)	-179.3938
			D(17,13,16,20)	0.5352
			D(12,14,18,16)	-0.4381
			D(12,14,18,21)	179.9678
			D(19,14,18,16)	179.015
			D(19,14,18,21)	-0.5785
			D(13,16,18,14)	0.3876
			D(13,16,18,21)	179.9813
			D(20,16,18,14)	-179.5417
			D(20,16,18,21)	0.052

Thermodynamic properties of all forms of PCBMTSC have been presented in Table 4. It can be described as form B shows more reactivity due to less entropy and free energy values. Form F has been more reactive with more enthalpy value. Dipole moment value was high for form B hence more reactive. The free energy values follow the order A < B < C < D < E < F. The order of entropy with respect to all forms is B > A > F > C > E > D.

Mulliken charges on the atoms of all the forms of PCBMTSC were recorded and presented in the Table 5. The net charge on the molecular forms has been found to be zero. The highest negative charge has been distributed over chlorine, nitrogen and sulphur atoms.

The optimized geometric parameters of each of the form of PCBMTSC has been calculated for all the six forms but in this presentation only data for A form has been given in Tables 6. These parameters explain about the distances, bond angles and bond lengths of an atom with respect to an origin atom.

ISSN- 2394-5125 VOL 07, ISSUE 09, 2020

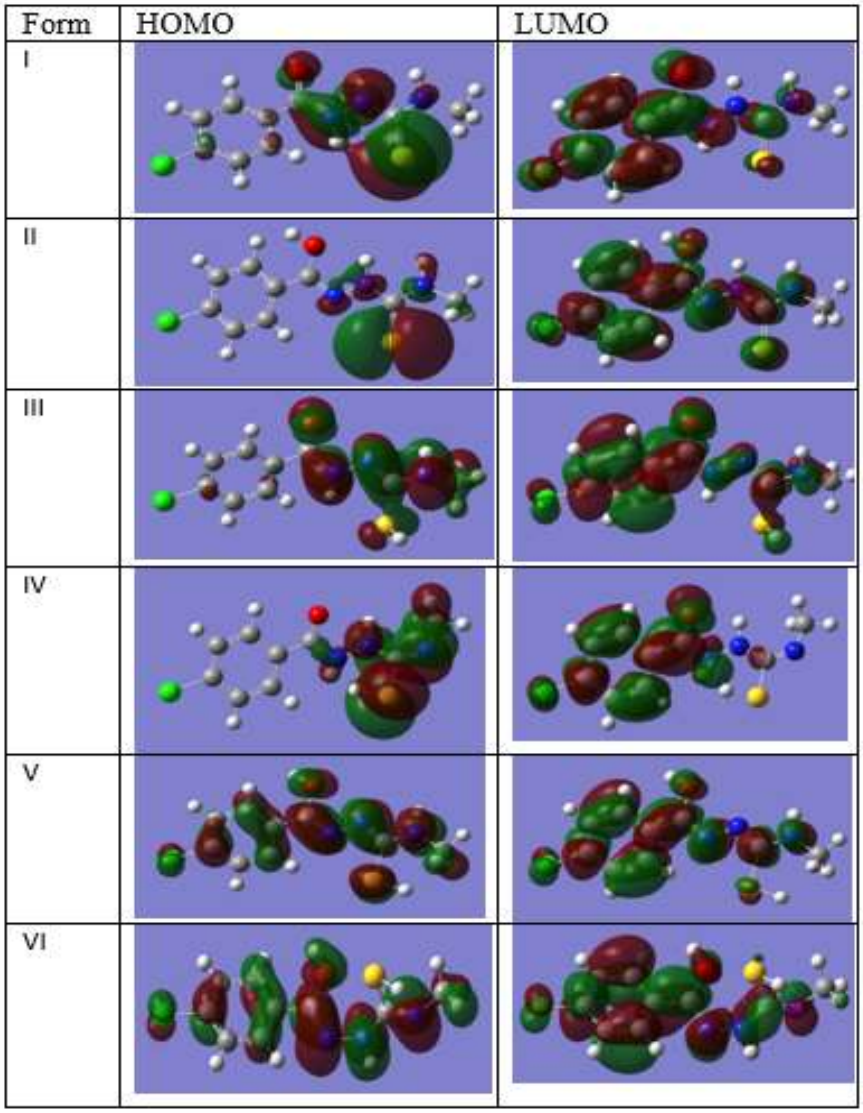

Fig 11: HOMO and LUMO of A-F forms of PCBMTSC

The HOMO and LUMO orbitals of PCBMTSC were diagrammatically represented in Figure 11. In forms A-D HOMO, LUMO lobes were oriented on to nitrogen, oxygen and sulphur atoms. In E and F forms HOMO, LUMO lobes were oriented on to all atoms leaving hydrogen atoms.

Table 7: Quantum chemical parameters of A-F forms of PCBMTSC

Parameters	A	B	C	D	E	F
E_{HOMO} (eV)	-0.23050	-0.20346	-0.22732	-0.24728	-0.20950	-0.220493
E_{LUMO} (eV)	-0.07064	-0.06835	-0.06181	-0.08042	-0.05842	-0.06503
ΔE_{gap} (eV)	0.15986	0.13511	0.16551	0.16686	0.15108	0.15546
IE (eV)	0.23050	0.20346	0.22732	0.24728	0.20950	0.22049
EA (eV)	0.07064	0.06835	0.06181	0.08042	0.05842	0.06503
Hardness (η) (eV)	0.07993	0.06755	0.08275	0.08343	0.07554	0.0777
Softness (*S*) (eV)	12.51094	14.80275	12.08386	11.9860	13.23801	12.86504
Electrophilicity (ω)(eV)	0.14181	0.13670	0.12627	0.16089	0.11877	0.13109
Chemical potential (μ) (eV)	-0.15057	-0.13590	-0.14456	-0.16385	-0.13396	-0.14276
Electronegativity (χ) (eV)	0.15057	0.13590	0.14456	0.16385	0.13396	0.14276

ISSN- 2394-5125 VOL 07, ISSUE 09, 2020

Additional electronic charge (ΔN max) (eV)	1.88377	2.01176	1.74690	1.96392	1.77336	1.83661

The quantum chemical descriptors of forms A-F of the compound were tabulated in the Table 7, which play a key role to understand the chemical reactivity and stability of the molecule. It has been revealed from the values that form B was better electron donor due to its low ionization potential value, soft and high reactivity corresponds to its low HOMO-LUMO energy gap and high softness value [28,29]. Form D with high electron affinity, high electrophilicity and high electronegativity values has been regarded as strong electrophile, better electron acceptor

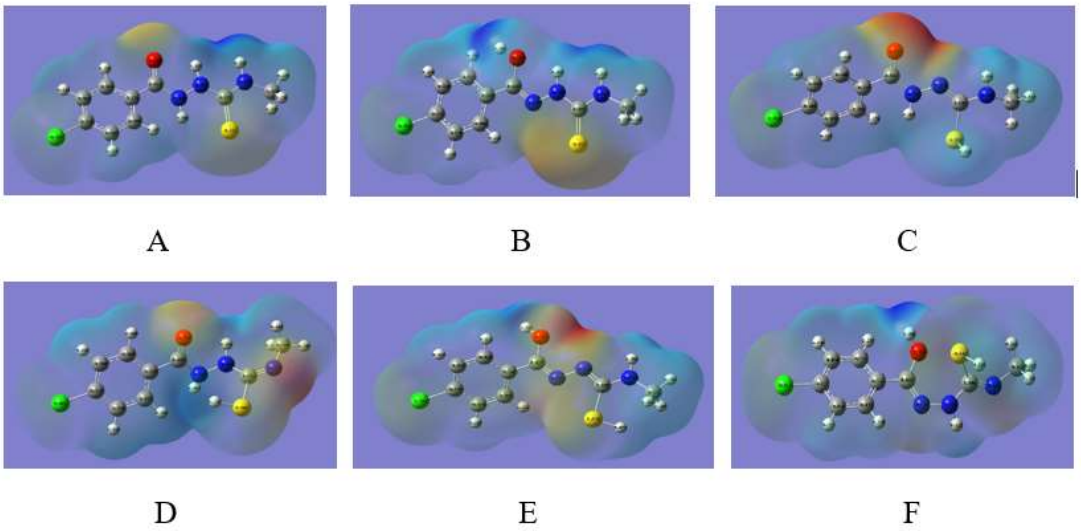

Figure 12. Molecular electrostatic potential surface of A-F forms of PCBMTSC

The MEP surface of keto enol and thione thiol tautomeric forms of PCBMTSC were shown in Figure 12. In the above forms the nucleophilic region has been localized to nitrogen atoms, methyl group, oxygen and sulphur atoms while electrophilic region has been localized over carbon and hydrogen atoms.

Equilibrium studies

The titration curves (Figure 13) resulted showed the formation of metal complex as the complex curve was below the free acid and ligand curves. The equilibrium studies [14] carried out in 70% v/v DMF-water medium at 303K and 0.1M KNO_3 ionic strength indicated the presence of one dissociable proton in PCBMTSC with pKa value 7.88 (Figure 14, table 8) and the data for obtaining dissociation constant has been presented in Table 14. The $\bar{n}$ values of Ni(II)-PCBMTSC system were in the range of 0.4-0.8 (Table 9) indicating the formation of 1:1ratio of metal complex in solution. The overall stability constant β for 1:1 Ni(II)-PCBMTSC complex was 3.43 (Figure 15) which indicates the formation of stable soluble complex in the solution.

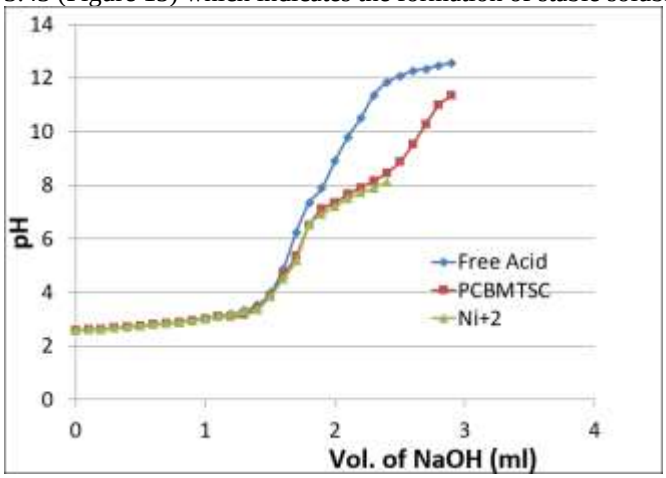

Figure 13. pH titration curves of Ni(II)-PCBMTSC binary system in 70% v/v DMF -water medium at 303K and 0.1M(KNO_3) ionic strength

ISSN- 2394-5125 VOL 07, ISSUE 09, 2020

Table 8. Data for obtaining dissociation constant of PCBMTSC

pH	$\bar{n}_A$	**Log** $(1-\bar{n}_A)/(\bar{n}_A)$
7.4	0.697	-0.366
7.5	0.662	-0.292
7.6	0.616	-0.205
7.7	0.578	-0.136
7.8	0.521	-0.036
7.9	0.492	0.032
8.0	0.464	0.063
8.1	0.412	0.154

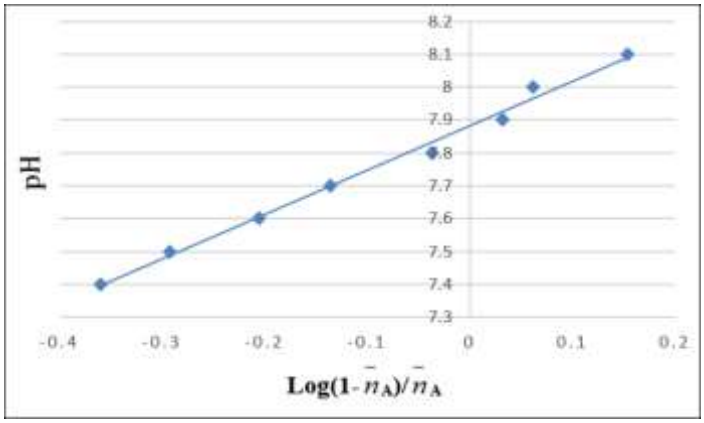

Figure 14. Linear Plot of Log [(1-$\bar{n}_A$)/ $\bar{n}_A$] Vs pH

Table 9. Data for obtaining formation constant of Ni(II)-PCBMTSC

$\bar{n}$	$\text{Log}(1-\bar{n})/\bar{n}$ (1:1)	pL
0.803	-0.61	3.33
0.732	-0.436	3.37
0.631	-0.231	3.39
0.528	-0.050	3.42
0.508	-0.014	3.45
0.481	0.033	3.48
0.464	0.069	3.50

ISSN- 2394-5125 VOL 07, ISSUE 09, 2020

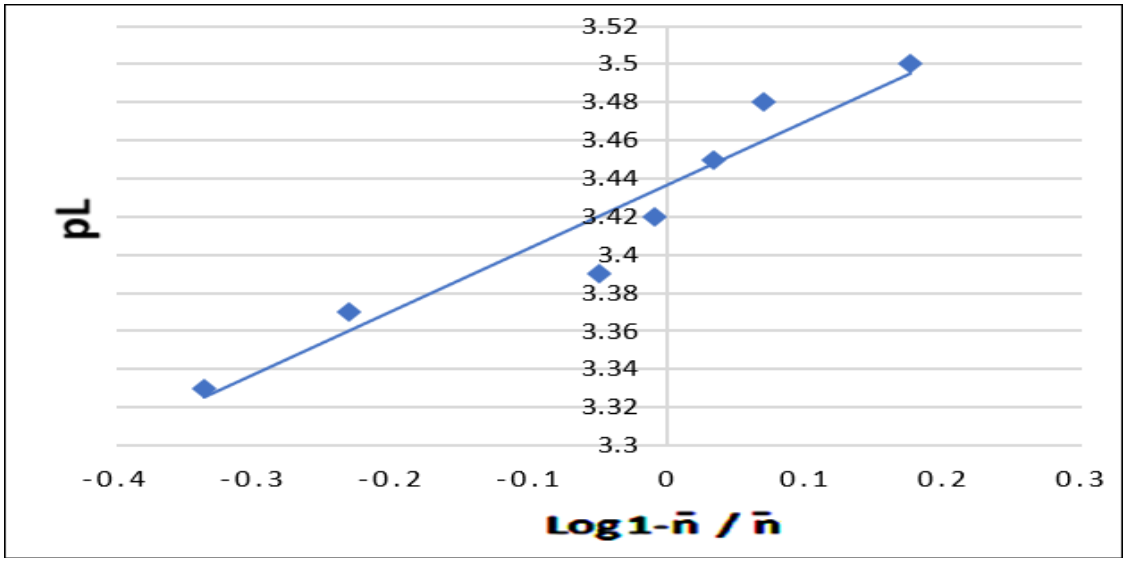

Figure 15. Plots of Log(1-$\bar{n}$)/$\bar{n}$ Vs pL of Ni(II)-PCBMTSC in 70% v/v DMF–Water medium

DNA binding studies

Electronic absorption spectroscopy studies

The interaction of calf thymus DNA with the metal complexes of PCBMTSC was evaluated using absorption intensity (Figure 16a, 16b). In this method absorbance of solutions was recorded by maintaining the concentration of complex constant and varying the DNA concentration. From the plots the DNA binding constant Kb has been calculated to 2×10^5 and 3.33×10^4 for complex 1 and complex 2 correspondingly. The values indicated hypochromism and intercalation mode of binding [30] in both the complexes.

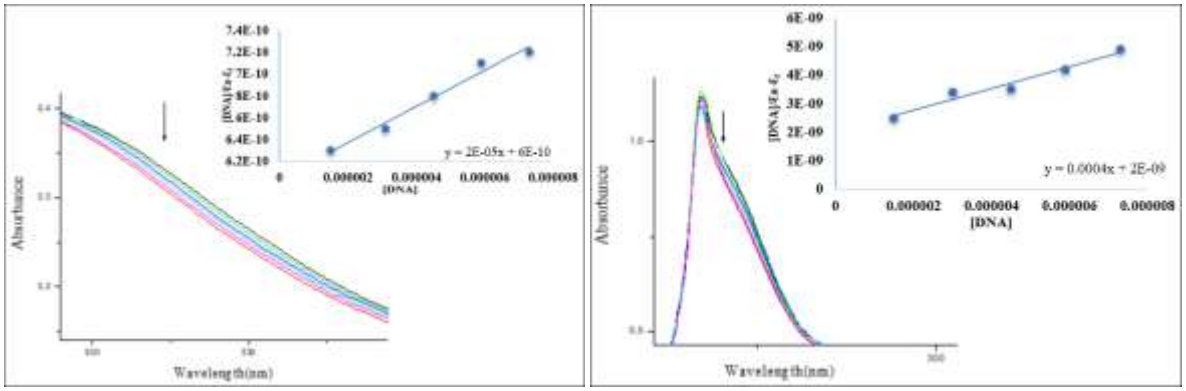

Fig.16a Absorption spectra of Ni(II)-PCBMTSC complex b. Cu(II)-PCBMTSC complex with increasing concentrations of CT-DNA [Inset: Linear plot of [DNA] Vs [DNA]/(ε_a-ε_f)]

Competitive fluorescence binding interaction

Fluorescence studies assist in studying the affinity of metal complexes towards DNA. This method gives us information about the extent of emission intensity reduction of Ethidium bromide and DNA adduct upon addition of increasing measure of complex solution. The ksv values of Ni(II)-PCBMTSC and Cu(II)-PCBMTSC complexes have been elucidated to $0.085\times10^3M^{-1}$ and $0.077\times10^3M^{-1}$ respectively (Figure 17a, b). This reveals the strong interaction between metal complexes and DNA.

ISSN- 2394-5125 VOL 07, ISSUE 09, 2020

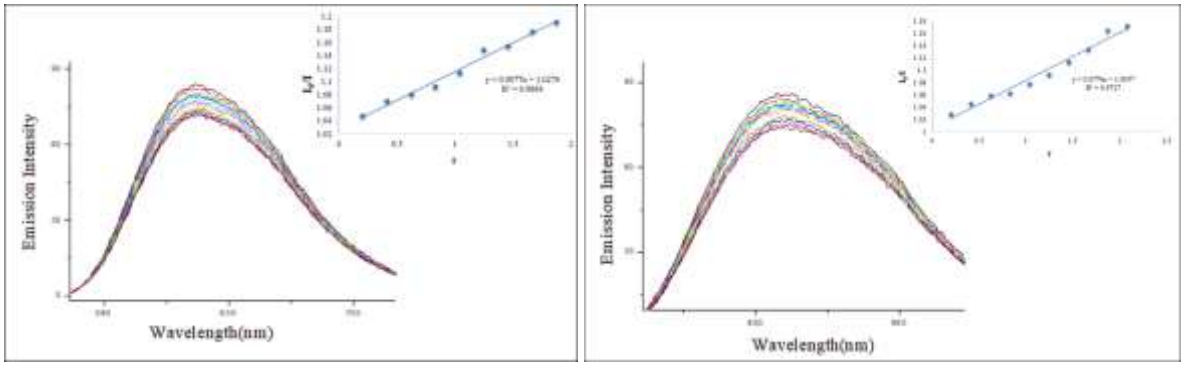

Fig. 17: Emission spectra of EB-DNA, in increasing concentrations of a. Ni(II)-PCBMTSC complex b. Cu(II)-PCBMTSC complex (Inset: linear stern -Volmer quenching curves)

Viscosity measurements

Viscosity values were measured using Ostwald's viscometer maintained at 30°C in thermostatic water bath. Viscosity of DNA depends on the change in the length of the double helical strand, which results when a small molecule interacts with strand. From the plots (Figure 18)) it is evident that viscosity of the solution increases with the increase in the concentration of the complex. This is indicative of intercalation mode of binding of metal complexes with DNA.

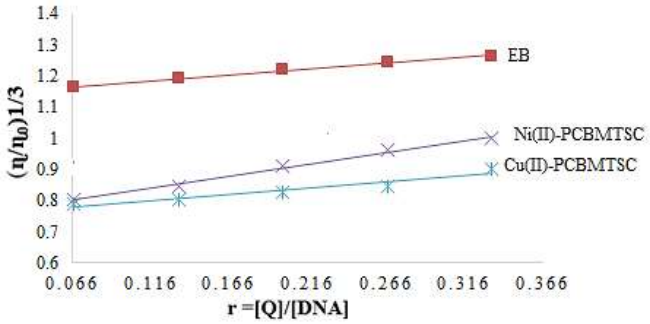

Fig.18: Effect of increasing concentrations of EB (red line), Ni(II)-PCBMTSC (purple line),Cu(II)-PCBMTSC (blue line) on the relative viscosity of CT-DNA.

DNA cleavage studies

Photocleavage studies have been carried out for complexes 1 and 2 of PCBMTSC using gel electrophoresis (Figure 19). When pBR322 plasmid DNA has been subjected to electrophoresis two forms were formed. They were fast migrating nicked (form II) and then slow migrating linear form (form III). In the presence of complexes plasmid DNA has been cleaved to nicked form indicating the partial degradation of DNA [31,32].

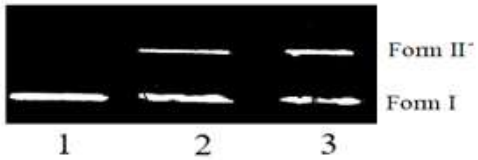

Figure 19. Photocleavage studies of pBR322 plasmid DNA by metal complexes. Lane 1, DNA control, Lane 2, DNA+ complex 1, Lane 3, DNA+ complex 2 respectively

Antimicrobial activity

Kirby -Bauer disc diffusion method has been employed to analyze the antimicrobial activity of the compound and its chelates. Zone of inhibition in mm of each compound has been measured using gentamycin as standard and represented graphically in Figure 20 and the values have been tabulated in Table 10. From the values it is evident that metal complexes show better activity against Gram -ve bacteria compared to compound as the complexes enhance the capability of compound to penetrate through cell membrane of infectious microorganisms.

Table 10. Antimicrobial activity of HL and complexes 1 and 2

ISSN- 2394-5125 VOL 07, ISSUE 09, 2020

Bacteria	PCBMTSC	Ni(II)-PCBMTSC	Cu(II)-PCBMTSC	Gentamycin
Bacillus	**7**	**6**	**7**	**15**
E-coli	**6**	**7**	**9**	**16**

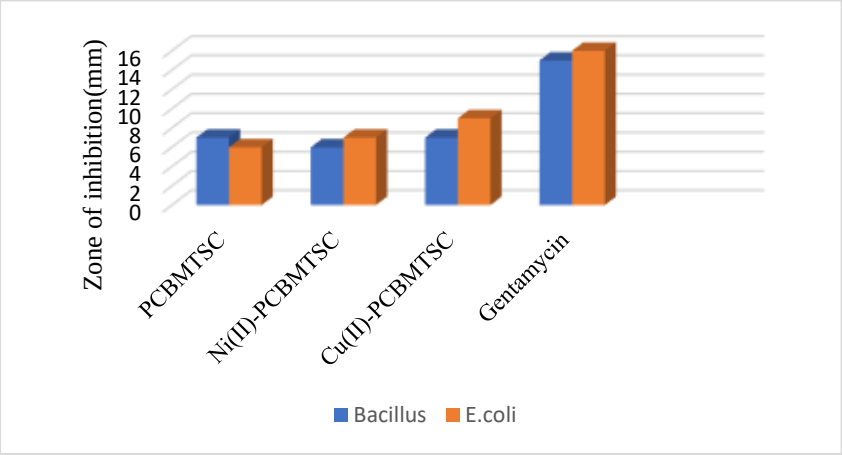

Figure 32. Graphical representation for antimicrobial activity of HL and its chelates at 50µg/mL concentration

Conclusions

PCBMTSC and its chelates with Ni(II) and Cu(II) ions have been synthesized and analyzed by several Spectro-analytical techniques which suggesedt distorted octahedral structure for both complexes. Computational studies describe form B of PCBMTSC to be most soft and highly reactive form. From equilibrium studies PCBMTSC has been regarded as monobasic in nature with one dissociable proton and formation of 1:1 Ni(II)-PCBMTSC system. DNA binding studies using electronic absorption studies, fluorescence studies and viscosity measurements reveal that complexes exhibit hypochromism with intercalation mode of binding. Gel electrophoresis indicates the cleavage of plasmid DNA to change into nicked form. Antimicrobial studies suggest that metal complexes display more activity than the compound (HL).

References:

1. P. Yogeeswari, D. Banerjee, P. Bhat, A. Thomas, M. Srividya and D. Shriram. Eur. J. Med. Chem.**,** vol. 46, p. 106-121(2011).
2. N. Siddiqui, O. Singh. Indian J. Pharm. Sci.**,** 65(4): 423-425 (2003).
3. A. Siwek, J. Stefanska, K. Dzitko and A. Ruszezak. J.Mol. Model.**,** vol. 18, p. 4159-4170 (2012**).**
4. A. Ameryckx, L. Thabault, L. Pochet, S. Leimanis, JH. Poupaert, J. Wouters , B. Joris, F. Van Bambeke and R. Frederick . Eur. J. Med. Chem.**,** vol. 159, p. 324-338 (2018).
5. A. R. Bhat, F. Athar, R. L. Vanzyl, C. T. Chen. and A. Azam. Chem. Biodivers., 5, 764-776 (2008).
6. Modern Theoretical Chemistry, A. Veillard, J. Demuynck, in H. F. Schaeffer, , 111 ed., Plenum Press, New York, 4, **1977**, 187.
7. M.P. Brahmbhatt, Sharma Sangita, J.J. Vora and J.D. Joshi Ultra Science**,** 14(2):262-265 (2002)**.**
8. F. M. Richards, H. M. Wyckoff and N. M. Allewel, Neurosciences**,** 901(1969**)**
9. A.N.M.A. Alaghaz, M.E. Zayed and S.A. Alharbi, J. Mol. Struc.**,** 182, 62-79 **(**2015).
10. M. Shanker, American Journal of Biological and Pharmaceutical Research**,** 3(2), 83-89 (2016).
11. Seijukubota and Masayuki Uda, Chem. Pharm. Bull. 23(5), 955-966, (1975).
12. Hanane Tabbi, Tahar Abbaz, Amel Bendjeddou and Didier Villemin, Int. J. Pharm. Sci. Rev. Res. 47 (2), November-December, Article No.24, p. 133-141 (2017).
13. Mohammad Jahidul Islam, Ajoy Kumer, Nuruzzaman Sarker, Sunanda Paul and Afroza Zannat. Advanced Journal of Chemistry, section A, 2(4), 316-326 (2019).
[35] K. Fukui, *Science* 218, **1982**, 747-754. https://doi.org/10.1126/science.218.4574.747
14. H.M. Irving and H.S. Rossetti, J. Chem. Soc.**,** 2904 (1954) .https://doi.org/10.1039/JR9530003397
15. A. Wolfe A,G.H. Shimer and T. Meehan. Biochemistry, vol. 26, p. 6392 (1987).
16. P. Satyadevi, P. Krishnamoorthy, E. Jayanthi, R.R. Butorac, A.H. Cowley and N. Dharmaraju, Inorganic Chimica Acta.**,** vol. 384, p. 83-96 (2012).
17. K.G. Strothkamp, and R.E. Strothkamp. J.Chem.Educ.**,** 71(1):77-79 (1994).
18. J.R. Lakowicz and G. Webber, Biochemistry.**,** 4161 (1973).

ISSN- 2394-5125 VOL 07, ISSUE 09, 2020

19. M.K. Jain, Journal of Biochemical and Biophysical methods**,** 9(2):181 (1984).
20. R. Punith, A.H. Hegde and S. Jaldappagari, Journal of Fluorescence.**,** vol. 21, p. 487-495. **(**2011).
21. A. Castineiras, G. Alzuet, J. Borras, J.L. Garcia-Gimenez, M. Gonzales-Alvarez and M.J. Liu-Gonzales, Inorg. Biochem.**,** vol. 103, p. 243-255 (2009).
22. B. Biswas, M. Mitra, A. Pal, A. Basu, S. Rajalakshmi, P. Mitra, N.A. Alkalde, G.S. Kumar, B.U. Nair and R. Ghosh, Ind. J. Chem.**,** 52A, 1576-1583 (2013).
23. P. R. Reddy and A. Shilpa, Indian Journal of Chemistry - Section A Inorganic, Physical, Theoretical and Analytical Chemistry.**,** vol. 49, no. 8, pp. 1003–1015 (2010).
24. S. Chandra, S. Parmar, and Y. Kumar, Bioinorganic Chemistry and Applications, Volume (2009), Article ID 851316, https://doi.org/10.1155/2009/851316.
25. B.T. Thaker and R.S. Barvalia, J. Coord Chem., 63 (9), 1597 (2010)**.**
26. M. N. Sivasankaran Nair, D. Arish and J. Johnson, J. Saudi. Chem. Soc., 20,591 (2016).
27. Inorganic electronic spectroscopy 2nd edn ,A.B.P. Lever, Amsterdam; Elsevier **(1984)**.
28. S. Gunasekaran , RA. Balaji, S. Kumeresan, G. Anand and S. Srinivasan, J. Anal. Sci. Spectrosc. 53, , 149-160 (2008).
29. RG. Pearson, J. Org. Chem. 54, 1423-1430,(1989). https://doi.org/10.1021/jo00267a034
30. L. Nitha, R. Aswathy, N. Mathews, B. Kumara and K. Mohanan, Spectrochim. Acta A, 118, 154 (2014).
31. A. Saritha, CH. Venkata Ramana Reddy and B. Sireesha, Der pharma chemical., 9(2): 90-98 (2017).
32.N.Kavitha and P.V.Anantha Lakshmi, Journal of Molecular structure (2019), https://doi.org/10.1016/jmolstruc.2018.09.042.